Mon. Not. R. Astron. Soc. **000**, 000–000 (2008)

Broad-band gamma-ray and X-ray spectra of NGC 4151 and their implications for physical processes and geometry

Andrzej A. Zdziarski[1], W. Neil Johnson[2] and Paweł Magdziarz[3]
[1] *Copernicus Astronomical Center, Bartycka 18, 00-716 Warsaw, Poland, Internet: aaz@camk.edu.pl*
[2] *E. O. Hulburt Center for Space Research, Naval Research Lab, Washington, DC 20375, USA*
[3] *Astronomical Observatory, Jagiellonian University, Orla 171, 30-244 Cracow, Poland, Internet: pavel@camk.edu.pl*

1 February 2008

ABSTRACT

We study γ-ray observations of NGC 4151 by *GRO*/OSSE contemporaneous with X-ray observations by *ROSAT* and *Ginga* in 1991 June and with *ASCA* in 1993 May. The spectra are well modeled by thermal Comptonization and a dual neutral absorber. We also find, for the first time for NGC 4151, a Compton-reflection spectral component in the *Ginga*/OSSE data. When reflection is taken into account, the intrinsic X-ray energy spectral index is $\alpha \sim 0.8$ and the plasma temperature is ~ 60 keV for both observations, conditions which imply an optical depth of ~ 1. The X-ray spectral index is within the range, $\alpha \simeq 0.95 \pm 0.15$, observed from other Seyfert 1s. Also, the OSSE spectra of those and other observations of NGC 4151 are statistically undistinguishable from the average OSSE spectrum of radio-quiet Seyfert 1s. Thus, NGC 4151 observed in 1991 and 1993 has the intrinsic X-ray/γ-ray spectrum typical for Seyfert 1s, and the main property distinguishing it from other Seyfert 1s is a large absorbing column of $\sim 10^{23}$ cm^{-2}. We find no evidence for a strong, broad and redshifted, Fe Kα line component in the *ASCA* spectrum of 1993 May. Also, the Compton-reflection component in the *Ginga*/OSSE spectrum is a few times too small to account for the strength of the broad/redshifted line reported elsewhere to be found in this and other *ASCA* spectra of NGC 4151.
On the other hand, we confirm previous studies in that archival X-ray data do imply strong intrinsic X-ray variability and hardness of the intrinsic spectrum in low X-ray states. An observed softening of the intrinsic X-ray spectrum with the increasing flux implies variability in γ-rays weaker than in X-rays, which agrees with the 100 keV flux changing only within a factor of 2 in archival OSSE and *GRANAT*/SIGMA observations.
The relative hardness of the intrinsic X-ray spectrum rules out the homogeneous hot corona/cold disk model for this source. Instead, the hot plasma has to subtend a small solid angle as seen from the source of UV radiation. If the hot plasma is purely thermal, it consists of electrons rather than $e^{\pm}$ pairs. On the other hand, the plasma can be pair-dominated if a small fraction of the power is nonthermal.

Key words: galaxies: individual: NGC 4151 — galaxies: Seyfert — X-rays: galaxies — gamma-rays: observations — gamma-rays: theory

1 INTRODUCTION

NGC 4151 is a nearby Seyfert 1.5 galaxy at $z = 0.0033$. In spite of its proximity and the wealth of X-ray and γ-ray data accumulated over the last 20 years, the nature of its nucleus remains poorly understood. Although it is the brightest Seyfert in hard X-rays it appeared to be distinctly different from average Seyfert 1s. Its X-ray spectrum is highly variable in the 2–10 keV energy spectral index, $\alpha \sim 0.3$–0.8 (e.g. Yaqoob & Warwick 1991, hereafter YW91; Yaqoob et al. 1993, herafter Y93). This hardness of the X-ray spectrum contrasts typical Seyfert 1s, which have $\alpha \simeq 0.95 \pm 0.15$ on average (Nandra & Pounds 1994). Furthermore, no characteristic spectral upturn above ~ 10 keV due to Compton reflection from cold matter, typical for Seyfert 1s (Nandra & Pounds 1994), was found in X-ray spectra of NGC 4151 from *Ginga* (Y93).

In this work, we present and discuss results of the moni-

toring of NGC 4151 by the OSSE detector aboard *GRO* from 1991 to 1993. In 1991 June and 1993 May, the OSSE data can be supplemented by data in X-rays from *ROSAT*/*Ginga*, and *ASCA*, respectively. These data suggest the intrinisic X-ray/γ-ray (hereafter abbreviated as Xγ) spectrum which is relatively steady in both the shape and amplitude, in contrast with many earlier observations in X-rays. We also study the presence of a Compton-reflection component and the form of the Fe Kα line in the data. We also consider implications of archival Xγ data from *EXOSAT*, *Ginga*, and *GRANAT*.

After presenting the data, we consider their implications for physical processes in NGC 4151. We study Comptonization in the Xγ source as well the presence of $e^{\pm}$ pairs and nonthermal acceleration. From that, we obtain strong constraints on the parameters and geometry of the central region of NGC 4151.

2 X-RAY/GAMMA-RAY SPECTRA

We consider first two broad-band Xγ spectra combining observations by OSSE in 1991 June/July and 1993 May with contemporaneous observations in X-rays by *Ginga*/*ROSAT* and *ASCA*, respectively. Then we consider other available data from OSSE, *Ginga*, *EXOSAT*, and *GRANAT*.

2.1 Fitted Models

We use XSPEC v. 9.0 (Arnaud 1996) for spectral fitting. The quoted errors are for 90 per cent confidence limit based on a $\Delta\chi^2 = 2.7$ criterion (Lampton, Margon & Bowyer 1976). Note that this confidence range correspond to the probability that a fitted parameter is in this range regardless of the values of all other parameters of a model (e.g. Press et al. 1992). Model parameters are given at $z = 0.0033$.

We use thermal Comptonization of Lightman & Zdziarski (1987, hereafter LZ87) as the hard continuum model (see Appendix). The parameters of the model are the plasma temperature, kT, and the spectral index, α, of the low-energy asymptotic power law. The second parameter is used instead of the geometry-dependent Thomson optical depth, τ, of the plasma. As an alternative form of the continuum, we use a power-law spectrum with an exponential cutoff.

We allow for the presence of a Compton-reflection component in the spectrum, which arises when cold matter (e.g. an accretion disk) subtends a substantial solid angle as seen from the Xγ source (Lightman & White 1988). We use angle-dependent reflection Green's functions of Magdziarz & Zdziarski (1995) and allow the reflecting medium to be either neutral or ionized and with the same abundances as in the absorber (see below). The relative contribution of reflection is measured by the ratio, R, of the flux emitted towards the reflector to that emitted outward. Equivalently, $2\pi R$ gives the solid angle covered by the reflector as seen from the Xγ source, with $R = 1$ corresponding to an isotropic continuum source above a slab.

The continuum is modified by absorption. We use here a dual absorber model, i.e., the product of complete absorption (with the hydrogen column density N_2) and partial covering by neutral medium (with the hydrogen column N_1 and the covering factor $C_{\rm f}$; e.g. Weaver et al. 1994, hereafter W94). We use the opacities of Bałucińska-Church & McCammon (1992) and the abundances of Anders & Ebihara (1982). However, the ratio of the Fe abundance to that of Anders & Ebihara (1982), $A_{\rm Fe}$, is a free parameter.

As an alternative, we also consider an ionized ('warm') absorber (Halpern 1984). We use a model of Done et al. (1992) but with the abundances of Anders & Ebihara (1982) instead of those of Lang (1974). Also, the iron edge energies are corrected (P. Życki, private communication) from the approximate values of Reilman & Manson (1979) to those of Kaastra & Mewe (1993). The former authors employ the Hartree-Slater approximation, which is accurate to a few per cent only (e.g. their K-edge energy of neutral Fe is 6.9 keV instead of 7.1 keV). The corrected absorber opacities agree then with those of Bałucińska-Church & McCammon (1992) in the limit of zero ionization. We assume the absorber temperature of 10^5 K (Krolik & Kallman 1984). The ionization parameter is defined by $\xi = L/(nr^2)$, where L is the 5 eV–20 keV luminosity in an incident power-law spectrum and n is the density of the absorber located at distance r from the illuminating source.

NGC 4151 exhibits a strong soft excess component, whose complex nature is not fully understood (e.g. Warwick, Done & Smith, hereafter WDS95). We model it simply as a power law cut off at an e-folding energy, $E_{\rm s}$. Its value is fixed at $E_{\rm s} = 2$ keV, which provides good fits for both 1991 June and 1993 May data sets. The index of the soft power law, $\alpha_{\rm s}$, is allowed to be different from that in the hard X-rays, which was found necessary by WDS95. This difference rules out the origin of the soft excess solely due to scattering by warm electrons external to the Xγ source, which origin was proposed by W94. The soft component is absorbed by a neutral medium with the Galactic column density, $N_0 = 2.1\times10^{20}$ cm^{-2} (Stark et al. 1992), except for the 1991 June observation.

NGC 4151 also emits an Fe Kα line around 6.4 keV. We model it here as a Gaussian ($f_{\rm Fe}$) centered at $E_{\rm Fe}$ with a width of $\sigma_{\rm Fe}$, the total photon flux $I_{\rm Fe}$, and absorbed in the same way as the continuum.

For the dual absorber, the model has the form,

$$F(E) = e^{-\sigma N_0}\left\{e^{-E/E_{\rm s}} I_{\rm s} E^{-1-\alpha_{\rm s}} + \left(1 - C_{\rm f} + C_{\rm f} e^{-\sigma N_1}\right) e^{-\sigma N_2}\left[I_{\rm Fe} f_{\rm Fe}(E) + I_{\rm c} f_{\rm c}(E)\right]\right\}, \quad (1)$$

where E is the photon energy in keV, $f_{\rm c}$ represents the hard continuum including reflection, $I_{\rm c}$ is its 1 keV normalization, and σ is the bound-free cross section of neutral matter. In the case of ionized absorber, the two first factors in the second line of equation (1) are replaced by $e^{-\sigma_{\rm ion} N_1}$, where $\sigma_{\rm ion}$ is the bound-free cross section of ionized matter with the hydrogen column N_1.

2.2 June 1991

2.2.1 The data

NGC 4151 was observed by OSSE 1991 June 29–July 12. The observation was reported before by Maisack et al. (1993). The data used here have been obtained with the response matrix and calibration revised since then (see Johnson et al. 1996). The response revision has resulted in the $\sim$ 60–70

keV flux being about 10 per cent larger now. Also, the 50–60 keV channel data have been added.

The present data include estimated systematic errors. These systematics were computed from the uncertainties in the low energy calibration and response of the detectors using both in-orbit and prelaunch calibration data. The energy-dependent systematic error was estimated at a value of 3 times the computed uncertainty and was added in quadrature to the statistical errors prior to spectral fitting. For NGC 4151, this systematic error is ~ 12 per cent of the statistical error at 50 keV and decreases to less than 0.1 per cent above 130 keV.

Close in time to the OSSE observation, NGC 4151 was observed by *Ginga*, 1991 May 31–June 2 (Y93), and by *ROSAT*, 1991 May 31–June 1. The *Ginga* (top-layer only) and *ROSAT* data have been analyzed by WDS95. Here we use both the mid-layer and top-layer *Ginga* data (Turner et al. 1989), as recently calibrated for the Leicester *Ginga* database (D. Smith, private communication). The mid-layer and top-layer data are fully consistent with each other above 9 keV, and the mid-layer data are more accurate than the top-layer ones at $\gtrsim 15$ keV. We use *Ginga* data from a time interval overalapping with the *ROSAT* observation (see WDS95). Note that this subset differs from the *Ginga* spectrum 'b' (in the notation of Y93), which was used in previous fits by Zdziarski, Lightman & Maciołek-Niedźwiecki (1993, hereafter ZLM93) and Titarchuk & Mastichiadis (1994, hereafter TM94). In order to allow for residual calibration uncertainties, we have added a 0.5 per cent systematic error to the *Ginga* data (Turner et al. 1989), and a 2 per cent error to the *ROSAT* data (WDS95). We then fit jointly the 0.2–2 keV *ROSAT* data, the 2–22 keV *Ginga* top-layer data, the 9–24 keV *Ginga* mid-layer data, and the 50–1000 keV OSSE data.

In the models below, we take into account the contribution to the *Ginga* spectrum from the BL Lac 1E1207.9+3945, which is located ~ 5 arc min from the nucleus of NGC 4151 and is not resolved by *Ginga*. The BL Lac is resolved by *ROSAT* (WDS95), which observation yields a power law spectrum with $\alpha \simeq 1.1$ and a normalization implying an about 10 per cent contribution to the *Ginga* spectrum at 2 keV. (We arbitrarily assume the BL Lac power law is cut off exponentially with an e-folding energy of 300 keV; the value of this energy has negligible effect on our fits.)

2.2.2 Results

Our baseline model contains a hard continuum due to thermal Comptonization, a soft X-ray component, a dual absorber, and a Kα line with the energy and width of 6.4 keV and 0.1 keV, respectively (see Section 2.1). We first fix the Fe abundance at the solar value of Anders & Ebihara (1982). We obtain an inacceptable fit with $\chi^2 = 194/126$ d.o.f. There are very strong residuals in the 5–8 keV range, which form an apparent broad line between 5 and 6 keV and an edge around 7 keV, as shown in Fig. 1*a*. However, these systematic residuals disappear when the Fe abundance is allowed to vary (reaching $A_{\rm Fe} = 2.8^{+0.3}_{-0.3}$; cf. YW91; Y93), as shown in Fig. 1*b*. The reduction in χ^2 is very large, to $\chi^2 = 99/125$ (at the continuum parameters of $\alpha = 0.74^{+0.02}_{-0.01}$, $kT = 54^{+9}_{-6}$ keV). The residuals at $A_{\rm Fe} = 1$ are explained by the presence

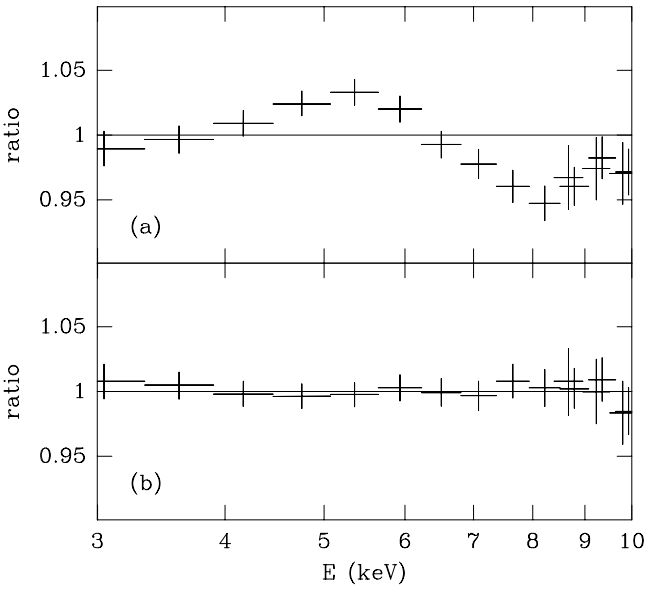

Figure 1. The 3–10 keV residuals to fits to 1991 June *Ginga* data. *(a)* The Fe abundance of Anders & Ebihara (1982). *(b)* The best fit Fe abundance. The broad ~ 5.5 keV feature apparent at the solar Fe abundance disappears now. See text.

of a strong K edge in the data, which causes the fitted local continuum to soften in order to account for the dip above the edge energy. This in turn gives rise to positive residuals below the edge and negative ones above it. The residual at ~ 6.5 keV is close to null because of compensation by an enhanced flux in the narrow ~ 6.4 keV line (~ 4 times stronger at $A_{\rm Fe} = 1$ than at free $A_{\rm Fe}$). Then the residuals between ~ 4 and 6.5 keV form a broad, line-like, feature.

In order to test the uniqueness of the obtained continuum shape, we also fit a power law with an exponential cut-off. We obtain a much worse fit, with $\chi^2 = 112/125$ d.o.f., for $\alpha = 0.56$, the e-folding energy of $E_{\rm c} = 121$ keV, and $A_{\rm Fe} = 3.5$. The model fits both *Ginga* and OSSE data worse than the thermal-Compton model. (The value of α is lower than that for the Comptonization model because of the different shapes of high-energy cutoffs of the two models fitted to the OSSE data.) Since the cut-off power-law model both gives a worse fit as well as it does not correspond to any physical process for the obtained parameters (see Section 3.1), we do not consider it any more.

We then compare our fits with the dual neutral absorber to those with a warm absorber and a soft X-ray component of the same form as for the dual absorber (see Section 2.1). We use thermal Comptonization for the hard continuum and allow for variable $A_{\rm Fe}$. We obtain a fit with a harder intrinsic power law and much worse statistically than that for the dual absorber; $\chi^2 = 155/126$ d.o.f. at $A_{\rm Fe} = 1.5$ with 4–10 keV residuals similar to those for the dual absorber at $A_{\rm Fe} = 1$. The warm absorber also gives a bad fit to the *ASCA* data set of 1993 May. These results support those of Warwick et al. (1996), who found that the time-variability pattern of soft and hard X-ray variability are difficult to reconcile with the ionized absorber model. Also, Kriss et al. (1995) have found from HUT data that the UV absorber consists of both high and low-ionization gas in the line of sight, which rules

out the simple model of WDS95 with the UV and X-ray absorbers being the same and the low neutral H column in the UV absorber explained solely by strong photo-ionization of the X-ray absorber. Therefore, we decided to use the dual absorber model throughout. We note that a good fit of the warm absorber model to the *ROSAT*/*Ginga* spectrum of NGC 4151 was obtained by WDS95 *before* the Fe ion edge energies have been corrected (see Section 2.1).

We then examine the presence of Compton reflection (Section 2.1). We assume first the inclination of $i = 65^\circ$, which is the minimum inclination allowed by *HST* observations of Evans et al. (1993). We find that adding a reflection component significantly improves the fit, reducing χ^2 by 10.5, to 88.6/124 d.o.f. This corresponds to the probability of 0.02 per cent that the fit improvement was by chance. The reflection fraction is $R = 0.43^{+0.23}_{-0.22}$. The spectrum is shown in Fig. 2*a* and the fit parameters are given in Table 1. We caution, however, that we do not directly see a hardening of the spectral slope above ~ 10 keV in NGC 4151 due to strong absorption, whereas such hardenings are seen in many other, less absorbed, Seyfert 1s (Nandra & Pounds 1994). Thus, the evidence for reflection in NGC 4151 is indirect, and the improvement of the fit may possibly be an artifact of our choice of the models for the continuum and absorber.

Reflection at $R = 0.43$ results in an increase of the fitted kT, from 54 keV to 88^{+56}_{-25} keV (but see Section 3.1), and an increase of the spectral index to $\alpha = 0.80^{+0.03}_{-0.03}$. The soft X-ray component is absorbed by $N_0 = 3.3^{+0.3}_{-0.3} \times 10^{20}$ cm^{-2}. The best-fit Fe abundance is lower when reflection is included, $A_{\rm Fe} = 2.2^{+0.4}_{-0.4}$, because a part of the K edge is now accounted for by the reflection component.

We note that the *Ginga* top-layer data alone are consistent with the presence of reflection ($R = 0.47$ gives the best fit), but $R = 0$ is within the 90 per cent confidence interval. Addition of both the *Ginga* mid-layer data and the OSSE data strongly narrows that confindence interval. This is due, in particular, to the mid-layer data being more accurate than the top-layer data above ~ 15 keV, where the relative contribution of the reflection component peaks.

We have re-fitted the alternative models of an exponentially cut-off power law and of a warm absorber (see above) including now Compton reflection. We confirm that they provide much worse fits than our baseline thermal-Compton, dual-absorber, model even when reflection is included. E.g. $\chi^2 = 102$ for the cut-off power-law model with reflection ($\alpha = 0.66$, $E_{\rm c} = 150$ keV, $R = 0.38$) and the dual absorber, i.e., $\Delta\chi^2 = 13$ with respect to the corresponding thermal-Compton model.

The relative reflection fraction depends on the viewing angle (Magdziarz & Zdziarski 1995). The value of $i = 65^\circ$ (Evans et al. 1993) is rather uncertain. Therefore, we also consider two other inclinations, in particular $i = 20^\circ$ ($\cos i = 0.95$), which is the maximum inlination consistent with the Kα disk-line fits to *ASCA* data by Yaqoob et al. (1995, hereafter Y95). Inclinations of $\cos i = 0.2$ and 0.95 give $R = 0.76^{+0.40}_{-0.39}$ and $R = 0.24^{+0.14}_{-0.12}$, respectively, both with the same χ^2 as for $i = 65^\circ$. Note that the product $R \cos i$ (which determines the projected area emitting reprocessed UV flux, see Zdziarski & Magdziarz 1996), increases with $\cos i$; $R \cos i = 0.15$, 0.18, 0.23, for $\cos i = 0.2$, 0.42, and 0.95, respectively.

We then examine the effect of ionization of the reflector. We model it in the same way as ionization of the warm absorber (see Section 2.1). We obtain $\xi = 0^{+65}$ erg s^{-1} cm^{-1}, i.e., the reflector is close to neutral. Ionization reduces the fitted R, which becomes 0.32 only ($i = 65^\circ$) at the upper limit on ξ.

Furthermore, the amount of reflection depends on the overall metal abundance (with respect to H and He). Its best fit value equals 1.0 (with the free Fe abundance), with the 90 per cent confidence upper limit at 1.9. At this limit, the relative reflection is only about 10 per cent larger than for the solar abundances, e.g. $R = 0.27$ at $i = 20^\circ$. Thus, varying the overall metal abundance has only small effect on the amount of Compton reflection. We have also tested the effect of replacing the abundances of Anders & Ebihara (1982) by those of Anders & Grevesse (1989). The main difference between the two is the Fe abundance about 40 per cent higher in the latter. We obtain virtually the same spectral parameters and the values of χ^2 for both abundances. The Fe abundance with respect to that of Anders & Grevesse (1989) for the model thermal Comptonization and neutral reflection is $A_{\rm Fe} = 1.5^{+0.3}_{-0.2}$, which is just the range expected from rescaling the corresponding value in Table 1.

A Kα line is seen in the X-ray spectrum. Allowing the line width and energy to be free parameters, we obtain an insignificant reduction of $\Delta\chi^2 = -0.8$ at $E_{\rm Fe} = 6.2$ keV and $\sigma_{\rm Fe} = 0$ keV with respect to that at the fixed values of 6.4 keV and 0.1 keV, respectively. Thus, the data are consistent with the line being narrow and not redshifted. The equivalent width (EW) is 34^{+32}_{-33} eV (at $E_{\rm Fe} = 6.4$ keV and $\sigma_{\rm Fe} = 0.1$ keV and defined with respect to the hard continuum only). The predicted EW of the line from reflection at the fitted $R \simeq 0.4 \pm 0.2$ (for $i = 65^\circ$) is $\sim 60 \pm 30$ eV (George & Fabian 1991), which then constrains reflection to to $R \lesssim 0.4$. This constraint can be relaxed if the line is broader or the reflecting medium is moderately ionized (Ross & Fabian 1993), which possibilities are allowed by the *Ginga* data. In order to test the former possibility we add a second, broad and redshifted, Gaussian component to the model (Y95). For $E_{\rm Fe} = 5.7$ keV and $\sigma_{\rm Fe} = 0.7$ keV, which are typical values obtained by Y95, we obtain $\Delta\chi^2 = -0.3$ only, i.e., the data allow but do not require a second component of the line. The allowed EW of the broad line is 30^{+100}_{-30} eV, which allows R to be in the range from the continuum fit.

2.3 May 93

2.3.1 The data

NGC 4151 was observed by OSSE 1993 May 24–31. During that period, it was also observed by *ASCA* on 1993 May 25 (W94). OSSE observed no statistically significant variability of the 50–150 keV flux, with the test of the constant flux giving $\chi^2_\nu = 0.22$ for 7 d.o.f., and the average flux having 2.5 per cent dispersion. Thus the week-long OSSE spectrum can be used together with the single-day *ASCA* spectrum. The OSSE spectrum has been processed in the same way as that of 1991 June (see Section 2.2.1).

We have extracted the *ASCA* spectrum from the HEASARC archive using the *ASCA* software release of 1996 May (ASCAARF v. 2.61). This corrects some inaccuracies of

Table 1. Fit parameters for 1991 June and 1993 May observations for the thermal-Compton model with Compton reflection. I_c, I_s are in 10^{-3} cm^{-2} s^{-1} keV^{-1}, I_{Fe} is in 10^{-5} cm^{-2} s^{-1}; N are in 10^{22} cm^{-2}, and kT is in keV.

Obs.	kT	α	R	I_c	α_s	I_s	N_1	C_f	N_2	A_{Fe}	I_{Fe}
91	88^{+56}_{-25}	$0.80^{+0.03}_{-0.03}$	$0.43^{+0.23}_{-0.22}$	95^{+6}_{-6}	$1.4^{+0.1}_{-0.1}$	$2.5^{+0.1}_{-0.1}$	$7.3^{+1.2}_{-0.8}$	$0.74^{+0.09}_{-0.11}$	$4.3^{+0.7}_{-0.7}$	$2.2^{+0.4}_{-0.4}$	$10.0^{+9.0}_{-9.7}$
93	96^{+64}_{-27}	$0.77^{+0.03}_{-0.02}$	0.43f	86^{+8}_{-7}	$0.7^{+0.1}_{-0.1}$	$3.5^{+0.2}_{-0.1}$	$13.9^{+1.3}_{-1.1}$	$0.79^{+0.02}_{-0.03}$	$3.8^{+0.4}_{-0.4}$	$1.3^{+0.3}_{-0.3}$	64^{+14}_{-11}

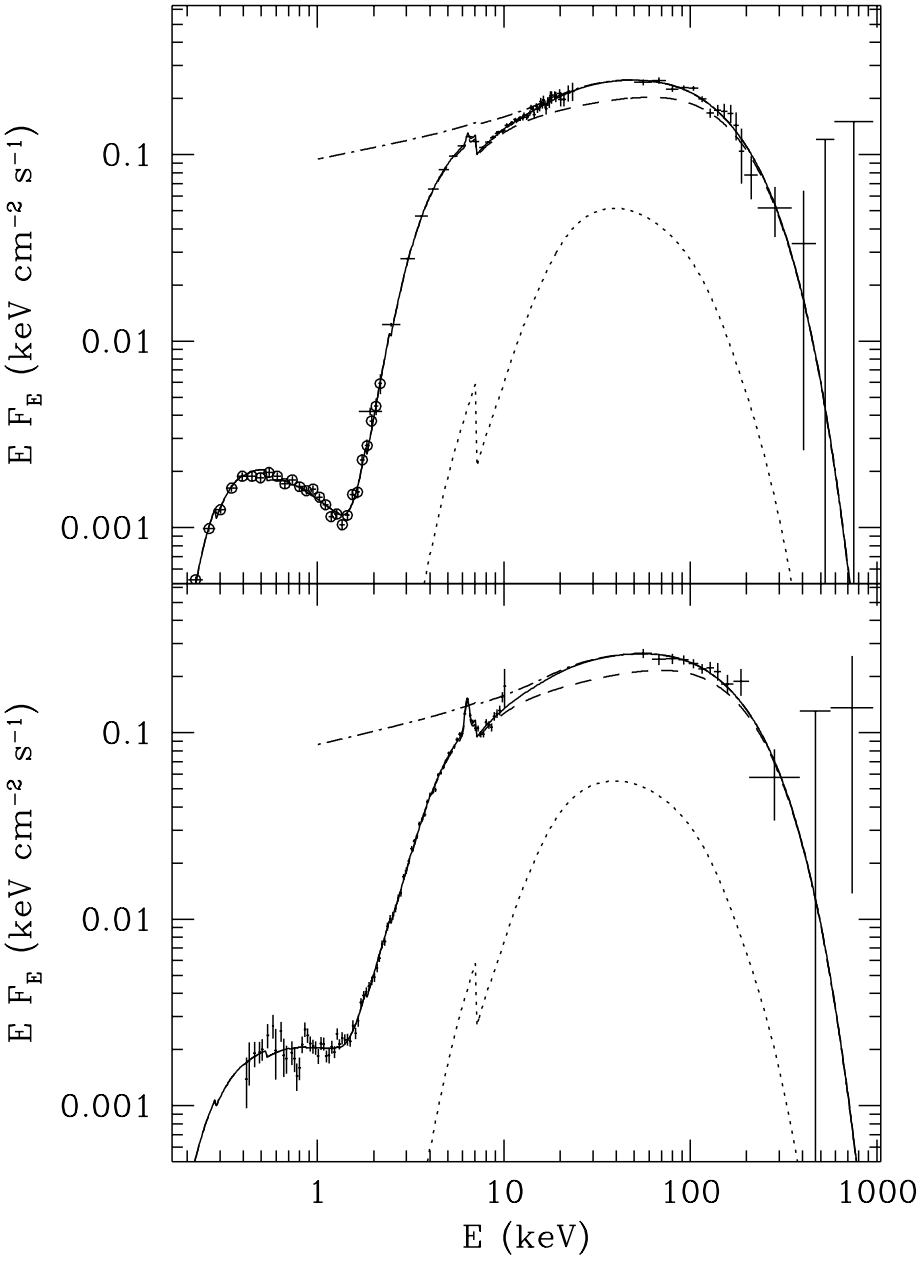

Figure 2. The Xγ spectra of NGC 4151 as observed *(a)* in 1991 June/July by *ROSAT*, *Ginga* and OSSE, and *(b)* in 1993 May by *ASCA* and OSSE. The dashed curves give the absorbed thermal Comptonization spectra, the dotted curves, the reflection components, and the solid curves give the models of the observed spectra. The dot-dashed curves give the unabsorbed continua (without the soft X-ray excess and the Kα line). The model parameters are given in Table 1. The plotted data have been rebinned for clarity, and the upper limits are 2-σ. The *ROSAT* data are marked with circles. The data from all 4 *ASCA* detectors have been co-added for plotting.

the detectors and telescope responses in the previous release (ASCAARF v. 2.53). In particular, the effective area of the GIS detectors is now about 20 per cent lower, and an instrumental broad spectral feature around 6 keV is now corrected for.

We used the standard data-screening criteria to select good data (see W94). The extraction of SIS data was done in rectangular regions covering parts of the chips 1 and 3 for SIS0 and SIS1, respectively. This maximized the usable SIS count rate from the observation, which was done in the 4-CCD mode with the source off-center (see W94). Still, a relatively large number of counts could not be recovered, which significantly reduced the the normalization of the obtained SIS spectra and rendered it unreliable (as noted by W94). Therefore, we use the GIS spectra (as corrected in the ASCAARF v. 2.61) for the absolute normalization. We note that the current GIS spectra yield the 8–10 keV fluxes about 1.2 times those obtained with the previous *ASCA* software (used, e.g. in Y95).

In fitting, we use the 0.4–10 keV SIS data, 0.8–10 keV GIS data, and the 50–1000 keV OSSE data. The *ASCA* data are rebinned to have at least 20 counts per bin, as required for the validity of the χ^2 statistics. Each of the four *ASCA* data sets is allowed to have free overall normalization, and the normalization of the OSSE data is tied to the average normalization of GIS2 and GIS3. Note that the *ASCA* data do not include systematic errors, which results in a relatively high χ^2_ν.

2.3.2 Results

We use the same models as in Section 2.2 to the combined *ASCA*/OSSE data. We first fit the model with thermal Comptonization, dual absorber, a soft X-ray component, free Kα line parameters, and no reflection. We obtain $\chi^2 = 1646/1683$ d.o.f. The hard continuum parameters, $\alpha = 0.72^{+0.03}_{-0.02}$ and $kT = 63^{+13}_{-13}$ keV as well its normalization, are very similar to the parameters of the corresponding model for the 1991 June data set (Section 2.2). We thus see that the intrinsic state of NGC 4151 in 1993 May is very close to that in 1991 June.

Since the 1991 June data show a Compton reflection component, we include it in the present data set as well. The energy range of the *ASCA* data precludes an independent determination of the strength of reflection and we simply fix it at the best-fit value for the 1991 June data, $R = 0.43$. The model yields the same $\chi^2 = 1646/1683$ d.o.f. as for $R = 0$. The continuum parameters are now $\alpha = 0.77^{+0.03}_{-0.02}$, $kT = 96^{+64}_{-27}$ keV with the 1 keV normalization of $I_{\rm c} = 8.6^{+0.8}_{-0.7} \times 10^{-5}$ cm^{-2} s^{-1}, which are indeed the same within the statistical uncertainties as the corresponding parameters of the 1991 June observation, see Table 1. The data and model are shown in Fig. 2*b*.

We have also tested a model with the ionized absorber instead of the dual neutral absorber, analogously to the 1991 June data (Section 2.2.2). We find that model gives a much worse fit, with $\Delta\chi^2 = +128$ (at free $E_{\rm s}$ and the absorber temperature of 10^5 K; $\Delta\chi^2 = +67$ at 10^6 K). The residuals for the fit resemble those shown in Fig. 1. Thus, ionized absorption does not provide a good model for the X-ray data.

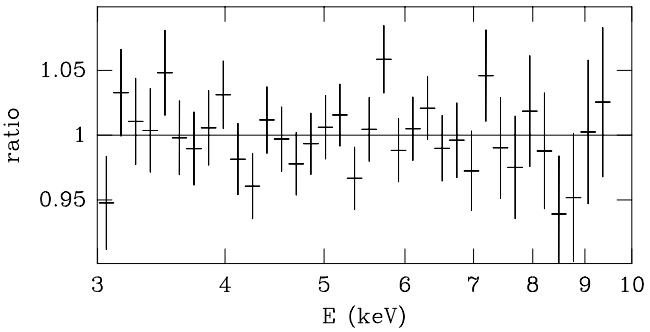

Figure 3. The 3–10 keV residuals to the single-line fit above 3 keV to 1993 May *ASCA*/OSSE data. No broad, redshifted component of the Kα line is seen. The data from all 4 *ASCA* detectors have been added for plotting. See Section 2.3.2.

We find that the soft X-ray component in the spectrum of NGC 4151 is also consistent with being constant. The 0.5–1 keV flux is $\simeq 2 \times 10^{-12}$ erg cm^{-2} s^{-1} for both 1991 June and 1993 May observations. Note that contributions from extended soft X-ray emission (e.g. Morse et al. 1995) are different for each of the observations, which accounts for at least some of the small differences in the soft X-ray spectra seen in Fig. 2. We also note that although the soft X-ray excess in the *ROSAT*/ginga data (Section 2.2) can be fitted by bremsstrahlung better than by a power law (WDS95), bremsstrahlung at the same temperature provides a bad fit to the soft X-ray excess in the *ASCA* data ($\Delta\chi^2 = +58$). On the other hand, the model of equation (1) provides a good description of both data sets.

The two spectra strongly differ, however, in absorption and the strength of the Kα line. The column density of the partial coverer is now about a factor two larger, $N_1 \simeq 1.4 \times 10^{23}$ cm^{-2}, and the Kα line is now much stronger, EW $= 250^{+50}_{-50}$ eV, than in 1991 June. This is suggestive of the difference in the line strength between the two spectra, ΔEW $\simeq 200$ eV, being due to emission by the additional absorption column in 1993 May (Makishima 1986). The parameters of the line are $E_{\rm Fe} = 6.36^{+0.03}_{-0.04}$ keV, $\sigma_{\rm Fe} = 0.16^{+0.07}_{-0.09}$ keV. This corresponds to the range of cloud velocities of $\Delta v \simeq 18^{+8}_{-10} \times 10^3$ km s^{-1} (Lang 1974), which suggest clouds at $\gtrsim 10^2$ Schwarzschild radii.

On the other hand, Y95 has found that the Kα line in this observation is very broad and redshifted, which would suggest its origin from Compton reflection. As pointed out by Y95, NGC 4151 has a complex continuum shape, and the choice of the continuum model affects results regarding the line. In particular, the soft X-ray continuum is poorly understood, and our model of it is only phenomenological. Thus, we follow Y95 in constraining detailed fits of the Kα line to the range to ≥ 3 keV (but we use the OSSE data as a constraint on the continuum). We freeze $\alpha_{\rm s}$, $I_{\rm s}$, and N_2 (which determine the shape of the spectrum below 3 keV) at the values obtained by fitting the whole *ASCA* energy range (Table 1). The single-line fit now gives $\chi^2 = 1158/1231$ d.o.f., and the line parameters are similar to those above, $E_{\rm Fe} = 6.36^{+0.04}_{-0.04}$ keV, $\sigma_{\rm Fe} = 0.13^{+0.06}_{-0.04}$ keV, EW $= 220^{+50}_{-50}$ eV. (Other parameters of interest are $\alpha = 0.79$, $kT = 110$ keV, $A_{\rm Fe} = 1.5 \pm 0.3$.) Fig. 3*b* shows the resulting 3–10

keV residuals, with no systematic deviations in the 5–6 keV range. Indeed, adding a second Gaussian (with 3 free parameters) improves the fit by $\Delta\chi^2 = -3$ only, which is statistically insignificant. The parameters of the second line are $E_{\rm Fe} = 5.8$ keV, $\sigma_{\rm Fe} = 0$ keV (poorly constrained due to the fact that such a line is not required by the data), and EW $= 25^{+23}_{-23}$ eV, i.e., the redshifted line component is much weaker than the main one. Thus, the presence of a broad and redshifted line component with a strength comparable to that of the narrow component is *ruled out*. This contrasts with the result of Y95, who obtained a fit improvement of $\Delta\chi^2 = -26$ due to adding a broad and redshifted Gaussian with the equivalent width similar to that of the narrow line.

In order to find the cause of this difference in the results, we have repeated the above analysis of the line shape using the same PHA files and response files as those used by Y95. We are still able to obtain a satisfactory fit with our single-line model, which gives $\chi^2_\nu = 0.97$ in the 3–10 keV range, which is the same as χ^2_ν obtained by Y95 for their 2-line model. No residuals in the 5–6 keV are seen for that model. Adding a second Gaussian results indeed in a negligible fit improvement, $\Delta\chi^2 = -4$, similarly as in the case of our *ASCA* data. This shows that a major cause of the difference between our results and those of Y95 is the difference in the choice of continuum. We use a power law (see Fig. 6 in Section 3.1) attenuated by a dual neutral absorber with variable Fe abundance whereas Y95 has chosen an analytic function designed to reproduce a power law and an ionized absorber. A possible strong effect of changing the absorption law on the presence of a broad, redshifted, line is illustrated in Fig. 1. One difference between the results based on the two data sets is that the broad, redshifted, Gaussian fitted to the data of Y95 has EW = 180 eV, which is of the same order as the EW of the narrow line. Such a strong feature is ruled out in our current *ASCA* data. This is explained by the difference between the ASCAARF v. 2.53 and 2.61 (see Section 2.2.1).

However, most of the statistical evidence of Y95 for the presence of a strong broad-line component in NGC 4151 comes from 1993 December observation, with the exposure time of 41.2 ksec, compared to 15.5 ksec in 1993 May. Thus, our conclusions regarding the weakness of a broad line need to be confirmed by studying longer-exposure spectra, e.g. the 1993 December one. We also stress that other Seyferts with a broad line seen in the *ASCA* data, e.g. MCG –6-30-15 (Tanaka et al. 1995), have much less absorption than NGC 4151 and thus the shapes of their broad lines are very weakly dependent on details of absorption.

Finally, we note that the data above 3 keV are fitted with $A_{\rm Fe} = 1.5\pm0.3$, which is consistent with $A_{\rm Fe} = 2.2\pm0.4$ in 1991 June for $A_{\rm Fe} = 1.8$. Thus, $A_{\rm Fe} = 1.8$ is the Fe abundance consistent with our 2 sets of data. On the other hand, a change of fitted $A_{\rm Fe}$ may result from our idealized modeling of absorption as due to a dual neutral absorber.

2.4 Other Data

The 1991–93 OSSE observations of NGC 4151 show a remarkable constancy of its γ-ray flux with time (see Section 2.4.1 below). In the four OSSE observations, the 50–200 keV flux changed within ±10 per cent only. This is consistent with the constant intrinsic Xγ spectrum found in this work for the 1991 June and 1993 May observations. On the other hand, *Ginga* has shown strong intrinsic X-ray variability of NGC 4151 (YW91; Y93). Also, some previous experiments showed strong γ-ray variability (Perotti et al. 1981, 1991; Baity et al. 1984). Those γ-ray data, however, were obtained with relatively uncertain background subtraction and low signal-to-noise ratio. Thus, a question arises whether the γ-ray flux of NGC 4151 is indeed highly variable in general and the present approximate constancy is specific to the 1991–1993 epoch or, to the contrary, the γ-ray flux is almost constant universally? We attempt here to address this question by considering archival OSSE, *Ginga*, *EXOSAT* and *GRANAT* data from NGC 4151.

Table 2. Fit parameters for the OSSE data for NGC 4151 and the average spectrum of weaker radio-quiet Seyfert 1s (Sy1). The model is a power law with an exponential cutoff. $E_{\rm c}$ is the e-folding energy in keV, F_1 and F_2 are the 50–100 keV and 100–200 keV fluxes, respectively, in 10^{-4} cm^{-2} s^{-1}.

Obs.	$E_{\rm c}$	α	χ^2/dof	F_1	F_2
4	83^{+29}_{-22}	$0.28^{+0.30}_{-0.41}$	42/50	24	8.7
218	96^{+80}_{-30}	$0.57^{+0.47}_{-0.46}$	33/50	22	7.3
222	93^{+56}_{-33}	$0.30^{+0.42}_{-0.58}$	26/50	25	9.9
310	70^{+31}_{-22}	$0.24^{+0.41}_{-0.61}$	38/50	26	8.5
All	98^{+18}_{-14}	$0.33^{+0.21}_{-0.23}$	152/206	—	—
Sy1	75^{+12}_{-27}	$0.09^{+0.70}_{-0.81}$	46/50	—	—
Sy1+All	82^{+17}_{-13}	$0.31^{+0.20}_{-0.22}$	199/258	—	—

2.4.1 OSSE Data

All up to-date observations of NGC 4151 by OSSE are presented in detail by Johnson et al. (1996). Here we consider the data from four viewing periods (hereafter VP) until the end of 1993, namely 1991 June 29–July 12 1991 (VP 4), 1993 April 20–May 3 (VP 218), 1993 May 24–31 (VP 222), and 1993 December 1–13 [VP 310; from Warwick et al. (1996)].

All the data are well fitted by the thermal Comptonization model with reflection. However, we present here fit results with an exponentially cut-off power law (which fits the OSSE data alone equally well), in order to give a convenient representation of the γ-ray spectra. We stress that this phenomenological model should not be extrapolated below 50 keV, and that α cannot be interpreted as the X-ray spectral index implied by the data. Table 2 shows the fit results as well as the photon fluxes in 50–100 keV and 100–200 keV bands. We see that all the spectra are approximately compatible with the constant shape, and the fluxes vary within ±10 per cent only. All four data sets can indeed be well fitted ($\chi^2_\nu = 0.73$) with the same model at free normalization, as shown in Table 2.

Table 2 also shows the fit results for the average spectrum of all radio-quiet Seyfert 1s observed so far by OSSE with the exception of NGC 4151 (McNaron-Brown et al. 1996). That spectrum has been obtained using the current OSSE response. The response revision has resulted in an overall spectral softening with respect to the average Seyfert spectrum presented by Johnson et al. (1994). We see that the spectral parameters are consistent with those of NGC

4151 within the statistical uncertainties, as pointed out by Johnson et al. (1994). This can be quantified by fitting simultaneously the average Seyfert-1 spectrum together with all 4 spectra of NGC 4151. We find that the fit is then almost identical to that for the four NGC 4151 spectra at $\Delta\chi^2 < 1$ with respect to the χ^2 sum of the previous two individual fits. Thus, the OSSE data do not show a difference between the spectra of NGC 4151 and that of of the average Seyfert 1 sample. We have also obtained the same results for the average radio-quiet Seyfert-1 spectra based on smaller samples of objects observed by both *Ginga* and OSSE and by *EXOSAT* and OSSE (5 and 7 objects, respectively; Gondek et al. 1996).

2.4.2 Ginga and Exosat data

The 2 keV flux in *EXOSAT* and *Ginga* data changes by a factor of ~ 35 (Fig. 4; Pounds et al. 1986; Yaqoob, Warwick, & Pounds 1989; YW91; Y93). During the 1991–1993 monitoring of NGC 4151 by OSSE, four X-ray observations (Y93; W94; Y95; Warwick et al. 1996) show the 2 keV flux varying within a factor of ~ 5 in a lower part of the flux range observed by *EXOSAT* and *Ginga*.

If the γ-ray flux were universally close to constant, one should be able to fit the archival *Ginga* data together with the current OSSE data. We use both top-layer and mid-layer *Ginga* data. We first consider the data with the highest 2–10 keV X-ray flux, which were obtained 1990 May 15–16 (Y93). Fig. 4 shows the fit of the thermal Comptonization model. For models in this section, the soft excess component is fixed at the shape obtained for 1991 June data (see Table 1), and the column N_2 is constrained to $\geq 10^{22}$ cm^{-2} to avoid the hard X-ray continuum to appear below ~ 1 keV (see YW91). We use the OSSE 1993 May 24–31 data, which have the highest 50–200 keV flux. We obtain $\alpha = 0.84^{+0.04}_{-0.03}$ and $kT = 78^{+48}_{-17}$ keV at $\chi^2 = 84/104$ d.o.f., i.e., the data are very well fitted by the model. Thus, the highest observed X-ray and γ-ray states are compatible with each other. There is no reflection ($R = 0^{+0.18}$ at $i = 65^\circ$ and $R = 0^{+0.08}$ at $i = 20^\circ$), which is compatible with the lack of a detectable Fe Kα line (EW $= 0^{+15}$ eV). (Fitting the *Ginga* data alone gives almost identical results for α and R.) The upper limit on a second broad and redshifted line (see Section 2.3) corresponds to EW $= 0^{+16}$ eV. The covering factor is about 0.3, which is much less than typical for NGC 4151 (Y93). The Fe abundance is $4.3^{+0.9}_{-1.0}$, which is not compatible with the range of $A_{\rm Fe} \sim 1$–2.6 found for other data considered here (see also Y93). Since we use this data set only to constrain the variability range, we do not attempt here to explain this peculiar behaviour.

Then we fit the *Ginga* data with the lowest X-ray flux, which was observed 1987 May 29–31 (YW91). The *Ginga* data are fitted with $\alpha = 0.54^{+0.15}_{-0.06}$ (for the assumed $kT = 60$ keV), $R = 0^{+0.30}$ for $i = 65^\circ$ ($R^{+0.15}$ for $i = 20^\circ$), and $A_{\rm Fe} = 2.1^{+0.5}_{-0.5}$ at $\chi^2 = 48/49$ d.o.f. There is a strong Kα line with EW $= 270^{+60}_{-80}$ eV. The spectrum is strongly absorbed, with the covering factor of about 0.8. When extrapolated above 30 keV, the *Ginga* data imply $EF_E(50\,{\rm keV}) = 0.12 \pm 0.02$ keV cm^{-2} s^{-1}, which is a factor of 2 below the lowest 50 keV flux in the OSSE data up to 1993 (1993 April 20–May 3), $EF_E = 0.24 \pm 0.01$ keV cm^{-2} s^{-1}, as shown in Fig. 4.

Interestingly, the two *Ginga* observations do not confirm the presence of continuum Compton reflection in NGC 4151. Furthermore, the flux in the Kα line varies less than the X-ray continuum, as well as it is larger for more absorbed spectra. This is inconsistent with the origin of most the line from reflection but rather suggestive of a substantial contribution from absorption by cold matter at a relatively large distance from the nucleus. Some Kα emission is then due to absorption of the continuum, and it is (i) averaged over the light-travel time across the absorber and (ii) stronger when absorption is stronger (Makishima 1986).

All X-ray spectra obtained by *EXOSAT* are below the spectrum of the highest *Ginga* state. On the other hand, the lowest X-ray states from *EXOSAT* obtained in 1984 April (Pounds et al. 1986) have 2–10 keV fluxes lower than that of the lowest *Ginga* state. There are two data sets, from April 8 and April 18–19. The spectrum with the lower flux (April 18–19) is indicated as uncertain (quality flag 2) in the *EXOSAT* archive. Thus, we use here the spectrum from April 8 (quality flag 4), which has the 2–10 keV flux only 10 per cent higher (although both spectra are similar). The data quality is, however, still insufficient to constrain the Fe abundance. Thus, we fix it at $A_{\rm Fe} = 2$ (see Table 1; Y93). Then a fit with a power law, dual absorber and the fixed soft excess yields $\alpha = 0.47^{+0.57}_{-0.33}$, and a strong K$\alpha$ line with EW $= 350$ eV, see Fig. 4. Although the implied 50 keV flux is poorly constrained due to the uncertain α, even the hardest power law allowed by the data yields $EF_E(50\,{\rm keV}) = 0.14$ keV cm^{-2} s^{-1}, which is a factor of ~ 2 below the lowest 1991–93 OSSE state, similarly to the lowest *Ginga* state.

2.4.3 GRANAT data

NGC 4151 was observed from 1990 July to 1992 November by the *GRANAT* satellite (Finoguenov et al. 1995). In particular, it was observed by the ART-P (below 30 keV) and SIGMA (above 30 keV) instruments on 1991 June 29 and July 11–12 , i.e., contemporaneously with the OSSE observation of 1991 June 29–July 12. The *GRANAT*, OSSE, and *Ginga* observations are compared in Fig. 5. We see that the OSSE and SIGMA data are consistent with each other. On the other hand, the ART-P data are somewhat above the corresponding *Ginga* data. The cause of that may be X-ray variability (since the *Ginga* data are from about a month earlier) as well as uncertainty in the relative calibration of the instruments. Still, the *Ginga* data match very well the OSSE data (see Fig. 2*a*), and the slow variability seen in the OSSE range (Section 2.4.1) is compatible with the spectrum above 50 keV during the *Ginga* observation being indeed at the level measured one month later.

SIGMA has observed an almost constant γ-ray flux from NGC 4151 during 4 out of 5 observations (Finoguenov et al. 1995). During those observations, EF_E at 100 keV was $\sim 0.16 \pm 0.05$ keV cm^{-2} s^{-1}. In 1991 November, the flux of 0.30 ± 0.04 keV cm^{-2} s^{-1} was observed. The corresponding range in the 1991–93 OSSE observations is 0.18 ± 0.01 to 0.25 ± 0.01 keV cm^{-2} s^{-1}. Thus, although the SIGMA data by themselves indicate stronger variability than the OSSE data, the two data sets are consistent with each other within measurement errors.

Summarizing, the *EXOSAT*, *Ginga* and *GRANAT* re-

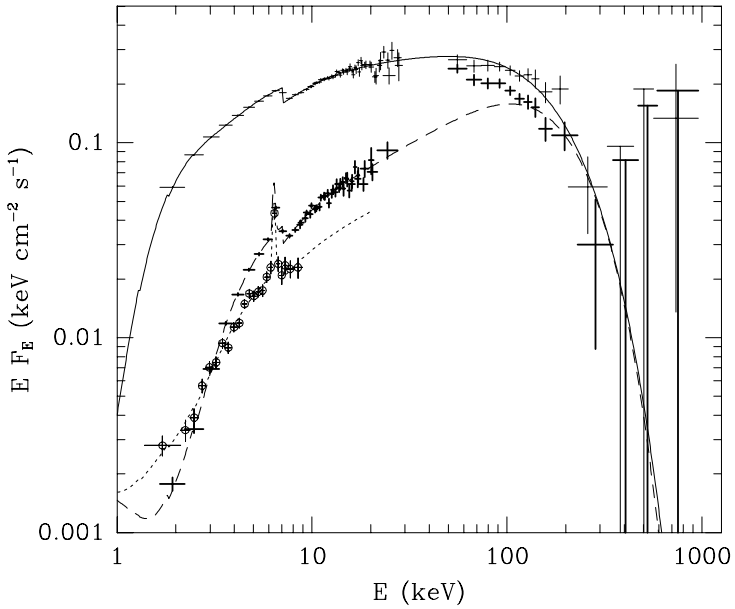

Figure 4. The range of X-ray states of NGC 4151 seen by *Ginga* (thin and thick crosses at < 30 keV) and *EXOSAT* (circled crosses) together with the range of γ-ray states seen by OSSE (not simultaneous; thin and thick symbols above 50 keV). The solid curve represents the thermal Comptonization model, which fits well the combined highest Xγ data. The dashed and dotted curves represent fits of the same model to the lowest *Ginga* and *EXOSAT* data, respectively, which both imply ~ 50 keV fluxes below the range seen by OSSE. See text.

sults strongly suggest that the fluxes between 50 and 100 keV vary at least within a factor of about 2, which is more than the range observed by OSSE in 1991–93. The strongest prediction is that of $EF_E(50\,\mathrm{keV}) \simeq 0.12 \pm 0.02$ keV cm^{-2} s^{-1} from extrapolation of the lowest *Ginga* spectrum, which EF_E is factor of 2 below the lowest 1991–93 OSSE flux of 0.24 ± 0.01 keV cm^{-2} s^{-1}. This is fact is confirmed by OSSE observation of a low > 50 keV state in 1995 (Johnson et al. 1996).

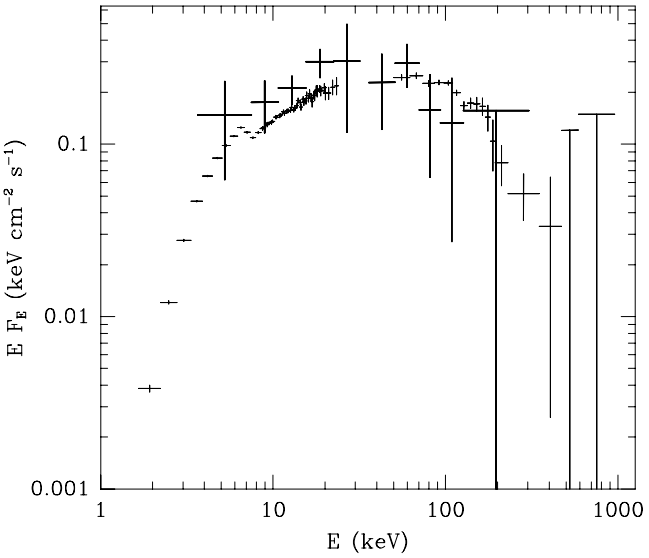

Figure 5. Comparison of observations of NGC 4151 by *GRANAT* 1991 June 29 and July 11–12 (thick symbols), by OSSE June 29–July 12 (thin symbols above 50 keV), and by *Ginga* May 31-June 1 (thin crosses below 30 keV).

3 THEORETICAL IMPLICATIONS

3.1 Source parameters and geometry

Our thermal Comptonization model uses α and kT as free parameters. The plasma optical depth, τ, is geometry-dependent. To determine it accurately for a uniform spherical source, we use a Monte Carlo method (see Appendix). We will use throughout the continuum parameters derived for 1991 June as the parameters for 1993 May are very similar, see Table 1.

We find that the spectrum observed in 1991 June (with $\alpha = 0.80$ and $kT = 88$ keV) corresponds to that from Componization in a uniform sphere (with a uniform distribution of seed-photon sources) with $kT = 61$ keV and $\tau = 1.3$. The temperature is lower than that obtained from fittting because the Comptonization model is formally obtained under the assumption of $\tau^2 \gg 1$ whereas τ approaches unity now. Still, that model gives a very good description of the shape of the spectrum, albeit for a somewhat different temperature, as shown in Fig. 6. Thus, the fit results for kT in Table 1 need to be rescaled by about 2/3, similarly to the case of the approximation of emission from optically thin plasmas by a power law with an exponential cutoff (Zdziarski et al. 1994). (However, a power law with an exponential cutoff does *not* approximate emission from plasmas with $\tau \gtrsim 1$.) The agreement of the parameters of our model with those from Monte Carlo improves rapidly with increasing τ (see Appendix).

The plasma cloud is irradiated by soft photons providing seeds for Comptonization. We take the seed photons as

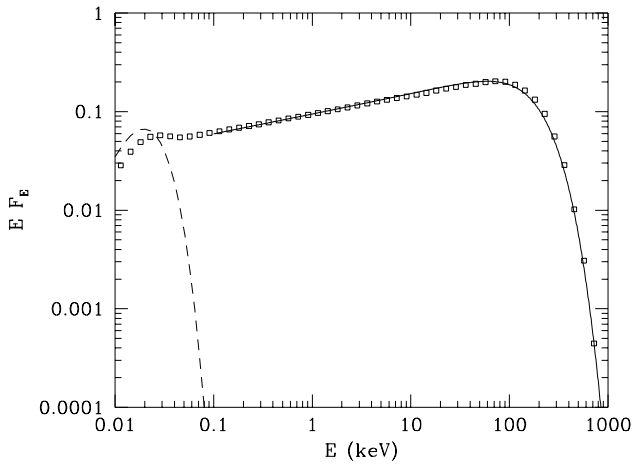

Figure 6. The Comptonization spectrum from a spherical plasma cloud with parameters corresponding to 1991 June. The solid curve gives the spectrum of the fitted continuum models and squares give results of our Monte Carlo simulations, see text. The model spectrum agree very well with Monte Carlo simulations. The dashed curve represents the seed diluted-blackbody photons with the temperature of 5 eV.

diluted blackbody at the temperature of 5 eV (Zdziarski & Magdziarz 1996; Kriss et al. 1995). The ratio of the Comptonized flux to the the soft flux irradiating the plasma is 13, i.e., the plasma is soft-photon starved. Some or all of the seed photons are due to reprocessing of the Comptonized, hard, radiation by cold matter, e.g. an accretion disk. We consider this effect here and find that the Xγ source cannot, contrary to a claim of TM94, form a homogeneous corona above the surface of an accretion disk.

A hot corona above a cold disk is cooled by soft photons emitted by the disk. The soft emission is due to both internal dissipation in the disk and reprocessing of hard radiation from the corona irradiating the disk. The cooling is minimized when all the dissipation occurs in the corona and none in the disk (Haardt & Maraschi 1993), which case we consider below. Anisotropy effects (Haardt 1993) are small at our derived plasma parameters and the corona emits photons approximately equally up and down (towards the disk). The down part is mostly absorbed and reemitted as the seed thermal UV radiation. The seed photons are upscattered, which self-consistently forms the Xγ corona emission. Since the seed photons are from the reprocessed ~ 50 per cent fraction of the corona photons emitted down, the observed Xγ luminosity, $L_{\rm X\gamma}$ (from the ~ 50 per cent of the corona photons emitted up), equals approximately the UV disk luminosity, $L_{\rm UV}$.

This condition is strongly violated in NGC 4151, in which $L_{\rm UV} \ll L_{\rm X\gamma}$ (see above). We have performed detailed Monte-Carlo calculations of a slab of hot electrons above a cold disk. For the spectral parameters for the 1993 June observation, we find the full slab thickness corresponds to $\tau \simeq 1.3$. The slab luminosity directed downward is 8.0 times the seed UV luminosity, $L_{\rm UV}^{\rm seed}$. Then we compute the integrated albedo of the cold disk, $A = 0.22$. Thus, the UV emission of the cold disk from reprocessing of the corona hard emission is $8(1-0.22) \simeq 6.2$ times the seed UV luminosity, i.e., $L_{\rm UV}^{\rm reprocessed} \simeq 6 L_{\rm UV}^{\rm seed}$. This strongly violates the energy balance condition, $L_{\rm UV}^{\rm seed} = L_{\rm UV}^{\rm reprocessed}$. The above discrepancy in the luminosities is much worse for the spectrum used by TM94, which is much harder than our intrinsic spectrum, and thus much more soft-photon starved. Furthermore, any power internally dissipated in the disk will worsen this discrepancy. Thus, the high-energy source in NGC 4151 cannot form a homogeneous corona, contrary to TM94. The discrepancy is due to TM94 both neglecting bound-free absorption in their albedo (which underestimates the absorbed fraction, $1-A$) and using formulae of Titarchuk (1994) derived under the assumption of $1-A \ll 1$ (while the actual $1-A \simeq 0.8$). (We also note that $\tau = 1.25$ given in TM94 as the optical depth of their hot corona is in fact the half-thickness of the corona on each side of the disk.)

Thus, the spectrum of NGC 4151 requires that the reprocessed UV radiation *returning* to the hot source(s) is reduced to ~ 0.2 with respect to that from a hot slab located above a cold slab. This soft-photon starvation can be achieved by geometry. The source can form one or more cloud at some height above the disk (e.g., Svensson 1996). For a suitable ratio of the height to the source size, only ~ 20 per cent of the reprocessed emission returns to the hot source. [Note that this geometry is different from the patchy coronae of Haardt, Maraschi & Ghisellini (1994) and Stern et al. (1995), in which Xγ sources are close to the disk surface and most of the reprocessed emission does return to the hot source.] On the other hand, the disk-corona geometry would imply a Compton reflection component with $R \sim 1$, which is more than that observed (unless for an edge-on orientation; Sections 2.2, 2.4.2). If the cold medium is Thomson-thick, the weakness of Compton reflection implies that the cold medium covers at most a $\sim 1\pi$ solid angle as seen from the hot source. A geometry compatible with both soft photon-starvation and reduced reflection is a hot inner disk and a cold outer disk (e.g., Shapiro, Lightman & Eardley 1976). Alternatively, the covering by the cold medium could be higher if the medium is Thomson-thin. Also, the hardness of the X-ray spectrum together with the relative weakness of Compton reflection is compatible with some configuration of hot and cold clouds with the mutual covering factors less than unity.

3.2 Electron-positron pairs

Here we examine if the hot source in NGC 4151 is dominated by $e^{\pm}$ pairs or by electrons. The pair production rate depends on the shape and the amplitude of the spectrum (Gould & Schréder 1967). On the other hand, the pair annihilation rate depends on the optical depth of the source. The two quantities are equal in pair equilibrium, which is established under most conditions even in variable sources (Svensson 1984).

We first assume that the Xγ emission is due to purely thermal Comptonization. We use the Comptonized spectrum with the parameters as for 1991 June (Table 1) to compute the total pair production rate (Gould & Schréder 1967). This rate scales with the size of the Xγ source, $r_{\rm X\gamma}$, as $r_{\rm X\gamma}^{-1}$. On the other hand, the pair annihilation rate scales as $r_{\rm X\gamma}$. Requiring the pair equilibrium we can solve for $r_{\rm X\gamma}$.

Assuming a spherical pure pair source and setting the average photon escape time to $r_{X\gamma}/c$ we obtain a value of $r_{X\gamma} = 2.2 \times 10^{11}$ cm. The Xγ luminosity is $L_{X\gamma} \simeq 5 \times 10^{43}$ erg s^{-1}, and the corresponding compactness parameter is very large, $\ell \sim 10^4$, where $\ell \equiv L_{X\gamma}\sigma_T/(r_{X\gamma}m_e c^3)$ (Svensson 1984). Thus, the required size of the pair source is rather small, and much less than the characteristic size of 10 Schwarzschild radii, $10r_S \sim 10^{14}$ cm implied by the black hole mass estimate of $\sim 4 \times 10^7 M_\odot$ of Clavel et al. (1987). Even the size inferred from the minimum possible mass from the condition of sub-Eddington luminosity during the highest states of the source (Section 2.4), $10r_S \sim 10^{13}$ cm, is still much more than the required size of the pair source. Furthermore, the Eddington limit is reduced for pair-dominated sources (Lightman, Zdziarski & Rees 1987), in which case $10r_S \gg 10^{13}$ cm. From the causality arguments it seems unlikely to release most of the bolometric luminosity (which is mostly in Xγ photons) in a region much smaller than the region in which most of the gravitational energy is released.

Thus, if the Xγ source in NGC 4151 is thermal, it consists most likely of e^- rather than $e^\pm$ pairs. Note that the situation in NGC 4151 differs strongly from that assumed in the models of Seyfert 1s of Stern et al. (1995). That study considers plasmas hotter and optically-thinner than that found here for NGC 4151, which results in $\ell \sim 10$ being already sufficient for the dominance of pairs.

On the other hand, ZLM93 considered a hybrid, thermal/nonthermal, model for NGC 4151, in which a small fraction of the electrons or $e^\pm$ pairs in the source is accelerated to nonthermal, relativistic, energies, but the bulk of the spectrum is still produced by thermal Comptonization. In the limit of zero nonthermal fraction (i.e., uniform heating of all electrons in the source), the model yields a pure thermal Comptonization spectrum. Acceleration has a two-fold role in the model. First, Compton scattering by nonthermal electrons as well as $e^\pm$ pair annihilation give rise to a weak tail on top of the thermal-Comptonization spectrum. [This contrasts the pure-nonthermal pair model proposed earlier to explain the *Ginga* spectra of typical Seyfert 1s (Zdziarski et al. 1990), in which *most* of the Xγ spectrum is due to nonthermal Comptonization.] Second, pair production by γ-rays in the tail can supply some or all thermal electrons/pairs in the source.

ZLM93 found that addition of a tail from nonthermal acceleration improves the fit to the *Ginga*/OSSE spectrum of 1991 June above ~ 200 keV. However, the plasma temperature in our present model (Table 1) is much above $kT \sim 40$ keV obtained by ZLM93. The present higher value is due to inclusion of Compton reflection, the revision of the OSSE response, as well as using a better absorber model. Consequently, our present model spectra (see Fig. 2) have the high-energy cutoff much more gradual than that of the spectrum of ZLM93. Thus, a spectral tail in our present model is not required.

However, an attractive feature of the hybrid model is that it can provide the electron optical depth needed for thermal Comptonization self-consistently. We find that the nonthermal compactness, $\ell_{nth} \equiv L_{nth}\sigma_T/(r_{X\gamma}m_e c^3)$ (where L_{nth} is the the nonthermal luminosity), required to produce pairs with the needed optical depth is $\ell_{nth} \simeq 10$, approximately independently of the total compactness. The nonthermal fraction, ℓ_{nth}/ℓ, is constrained to be small by the form of the cutoff in the γ-ray spectrum. For the *Ginga*/OSSE spectrum, we obtain $\ell_{nth}/\ell = 0.08^{+0.11}_{-0.08}$ in a model with nonthermal electrons accelerated to the Lorentz factor of 10^3. The best fit corresponds to a pure pair source with $\ell \simeq 140$ and $\Delta\chi^2 = -0.5$ with respect to the pure-thermal model, and the lower limit corresponds to the pure thermal-e^- source.

Thus, the source can be dominated by $e^\pm$ pairs if just ~ 10 per cent of the available power is released nonthermally. Such a situation is likely if the Xγ emission is from magnetic flares, in which reconnection can accelerate electrons. The characteristic compactness is $\ell \sim 10^2$, which corresponds to $r_{X\gamma} \sim 2 \times 10^{13}$ cm, which is then compatible with the estimates of the source size above. The compactness of $\ell \sim 100$ is super-Eddington for a *pure* pair source and thus we can rule out such a case. However, just ~ 10 per cent of protons in a pair-dominated source can provide the needed gravitational confinement of the plasma at that compactness (Lightman et al. 1987). Thus, the hybrid model described above is still a viable alternative to the pure thermal-e^- model.

4 DISCUSSION AND CONCLUSIONS

Observations discussed in this paper fall into two groups. First, we have found that the intrinsic spectra of NGC 4151 in 1991 June and 1993 May are the same within the observational uncertainties. This intrinsic spectrum is rather typical for Seyfert 1s (Nandra & Pounds 1994; Zdziarski et al. 1995) with an X-ray spectral index of $\alpha \simeq 0.8$, a Compton-reflection component, and the soft γ-ray spectrum with the shape not distinguishable from other Seyfert 1s. This is a new result for NGC 4151. On the other hand, archival data do show the intrinsic X-ray spectrum to be strongly variable, $\alpha \sim 0.3$–0.8, and very hard in low states, as well as with no reflection component at least in some states (confirming earlier results, e.g., YW91, Y93).

The Compton-reflection component found in the 1991 June *Ginga*/OSSE spectrum is relatively weak. It can be due to reflection from a disk (covering a solid angle close to 2π) if the nucleus of NGC 4151 is oriented close to edge-on. For a face-on orientation, the covering factor of the reflecting medium is only $\sim 0.2 \times 2\pi$. The fitted reflection fraction cannot be increased by varying either the Fe abundance, the overall metal abundance, or the ionization state of the reflector (Section 2.2). The shape of the continuum does not allow a determination of the inclination angle.

In spite of the similar continua in the 1991 and 1993 spectra, the Fe Kα line is much stronger in the 1993 observation, in which X-ray absorption is also stronger. The line in 1993 is narrow, and any broad and redshifted component (not required by the data) is constrained to $\lesssim 20$ per cent of the narrow component. The narrowness of the line in the 1993 observation together with the lack of the correlation between the strength of the continuum and that of the line suggests the origin of most the line photons from absorption rather than reflection. This is consistent with the relatively weak reflection in the 1991 June data.

The Xγ continuum is very well modeled by thermal Comptonization of soft UV photons by a plasma with $\tau \sim 1$ and $kT \sim 60$ keV (Section 3) and attenuated in X-rays by a

dual neutral absorber (which approximates absorption by a distribution of clouds). We have considered alternative models with an exponentially cut-off power law instead of the Comptonization spectrum as well as with an ionized absorber instead of the dual neutral absorber. We have found those alternative models describe the data much worse.

Another alternative model of the X-ray spectra in 1991 June and 1993 May has been proposed by Poutanen et al. (1996, hereafter P96). They assumed the intrinsic Xγ emission to be completely attenuated by an optically thick medium, and the observed emission to be from scattering towards our line of sight by an optically thin plasma, similarly as in the unified model of Seyfert 2s (e.g. Antonucci 1993). The shape of the observed spectrum is that of the intrinsic one at low energies, but it has an additional cutoff due to the Klein-Nishina scattering at high energies (e.g., Jourdain & Roques 1995). P96 consider two intrinsic emission models. One is a power law ($\alpha = 0.67^{+0.07}_{-0.05}$, which is harder than the Seyfert-1 average) with an exponential cutoff and reflection (as well as a soft X-ray component and a Kα line), and the other is a self-consistent disk-corona emission model (with $kT \simeq 200$ keV). Both models have high-energy cutoffs at several hundred of keV, which corresponds to the average spectrum, with $\alpha \simeq 0.9$, of Seyfert 1s (Zdziarski et al. 1995; Gondek et al. 1996). The models fitted to the *ROSAT*/*Ginga*/OSSE data of 1991 June (but without the *Ginga* mid-layer data) yield $\chi^2 = 120/110$ d.o.f. and 124/111 d.o.f., respectively. Those fits are much worse that these obtained by us (Section 2.2.2). Since P96 use a different model for the soft X-ray component and do not show their residuals or the contributions to χ^2 from each detector, it is difficult to establish the cause of the large difference in χ^2. However, the self-consistent disk-corona model plotted in P96 clearly overpredicts the spectrum around 20 keV, and it appears to give a worse fit to the OSSE data than our model does. P96 also fit their model to the *ASCA*/OSSE data of 1993 May. However, they use the SIS0 data with their own normalization, which is known to be incorrect (W94). That normalization is, in fact, a factor of ~ 2 less than that of the correct spectrum (Fig. 2*b*), and thus we do not compare our results for 1993 May with those of P96.

The difficulties of the scattering, Seyfert–2-like, model in fitting NGC 4151 appear to reinforce our conclusion that NGC 4151 as observed in 1991 and 1993 is intrinsically a Seyfert 1 with an average Xγ spectrum. The spectral index of $\alpha \simeq 0.8$ is within the 1-σ range of Seyfert 1s, 0.95 ± 0.15 (Nandra & Pounds 1994). Also, the OSSE spectra of NGC 4151 are statistically the same as the average spectrum of weaker radio-quiet Seyfert 1s observed by OSSE. The fact that the OSSE spectra of NGC 4151 are fitted with a high-energy cutoff energy less than that of the average Seyfert-1 Xγ spectrum is explained by a correlation between α and the cutoff energy. The correlation appears because harder X-ray spectra (such as of NGC 4151) need to be cut off faster than softer X-ray spectra in order to fit the same γ-ray spectrum.

The X-ray spectrum of NGC 4151 is too hard for the homogeneous disk-corona model of Haardt & Maraschi (1993) to apply. (We find that the disk-corona model applied to NGC 4151 by TM94 is in error.) We find the Xγ source in NGC 4151 subtends a small solid angle of $\sim 0.2 \times 2\pi$ as seen from the UV source (providing seed photons for Comptonization). This also rules out patchy corona models with the Xγ sources located on the surface of the disk. The possible geometries are either the Xγ sources at a large enough height above the surface of an accretion disk (e.g., Svensson 1996), a hot inner disk, or the UV-emitting cold matter in form of clouds.

Similar geometries have been considered by Zdziarski & Magdziarz (1996) as models for the UV/X-ray correlation observed in NGC 4151 by *EXOSAT* and *IUE* (Perola et al. 1986). Their transmission model explains the correlation as being due to the X-ray absorber re-emitting the absorbed X-ray power in the UV. The source parameters obtained here for the 1991 June and 1993 May data are consistent with that model. In particular, the width of the Kα line implies its origin at $\gtrsim 100$ Schwarzschild radii (Section 2.3.2), which is compatible with the UV response to varying X-rays delayed by $\lesssim 0.3$ day (Edelson et al. 1996) for the black hole mass of $\sim 10^7 M_\odot$. Unfortunately, no UV data exist for the Xγ observations studied here. The reflection model of Zdziarski & Magdziarz (1996) explains the correlation as UV-reemission of Xγ emitted towards a cold disk by a patchy corona. That model is independent of the corona geometry, and thus it is compatible with a photon-starved corona required by the spectra reported here. The model also requires that $R \cos i \gtrsim 0.15$, which condition is satisfied for the 1991 June observation (Section 2.2.2). We intend to test the models of Zdziarski & Magdziarz (1996) against the 1993 December *IUE*/*ROSAT*/*ASCA*/OSSE data (Warwick et al. 1996; Edelson et al. 1996).

The parameters of the Xγ source ($\tau \sim 1$, $kT \sim 60$ keV, Section 3.1) imply that pair production is negligible if the plasma is thermal (Section 3.2). On the other hand, a small fraction of the total power used to accelerate electrons to relativistic energies results in enough pair production for the plasma to be pair-dominated. Such acceleration may take place in magnetic flares, which are likely to be responsible for the formation of the disk corona. In both cases, the process responsible for the continuum emission is *thermal* Comptonization.

The conclusion of negligible thermal pair production differs from that of Stern et al. (1995), whose models are pair-dominated at $\alpha = 0.8$. Their models have $\tau \ll 1$ and $kT \sim 511$ keV, which allows them to be pair-dominated at a relatively low compactness. These models can fit the average OSSE spectrum of radio-quiet Seyfert 1s of Zdziarski et al. (1995) and Gondek et al. (1996). However, we are able to rule out $\tau \ll 1$ by direct fitting to the NGC 4151 spectrum, which is of much higher statistical accuracy.

We have also compared our 1991 and 1993 multi-wavelength observations with archival *Ginga* and *EXOSAT*, *GRANAT* and OSSE data. It appears that the intrinsic spectrum with $\alpha \simeq 0.8$ of 1991 and 1993 belongs to a high, soft, state of NGC 4151. The archival data also show a continuum of states limited by a low, hard, state with $\alpha \simeq 0.3$ (as found before by YW91 and Y95). The hardening of the X-ray spectrum with the decreasing X-ray flux results in the spectrum pivotting at a few hundred keV (YW91; Y93). This property allows the γ-ray spectrum, which breaks at ~ 100 keV, to vary within to a factor of a few only (as observed by OSSE and *GRANAT*), while the X-rays vary much more strongly (see Fig. 4). This behaviour can be modeled, for example, as due to a strongly-varying soft (UV) pho-

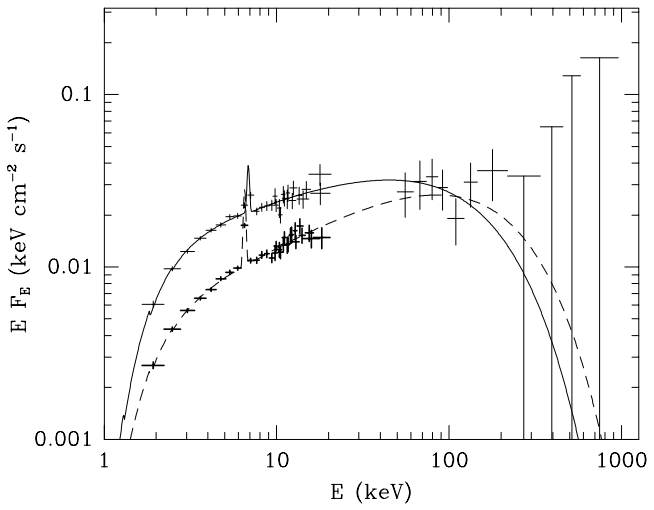

Figure 7. Spectra of MCG –5-23-16 (a Seyfert 2) from two *Ginga* and one OSSE observations (not simultaneous). The dashed and solid curves represent the fits with $\alpha \sim 0.4$ and 0.6, respectively. Such spectra are within the range seen in NGC 4151, see Fig. 4.

ton flux irradiating the Xγ source with a weakly-varying Xγ luminosity.

The hardness of the X-ray spectrum observed in some states of NGC 4151 by *Ginga* and *EXOSAT* is not unique among AGNs, and it is similar to that of, e.g., some Seyfert 2s (Smith & Done 1996). An interesting example is MCG –5-23-16. Two X-ray spectra from *Ginga* (Smith & Done 1996) are compared with the OSSE spectrum (Johnson et al. 1994) of that AGN in Fig. 7. The spectral indices are 0.44 and 0.62 (for a fit with a power law with an exponential cutoff) for the lower and higher X-ray state, respectively. This is within the range observed in NGC 4151 (Section 2.4.2). We see that the variable X-ray power law pivots around 100 keV. As a consequence, both *Ginga* spectra can be fitted together with the OSSE spectrum (not simultaneous). Also, the Kα line in MCG –5-23-16 has the constant line flux in the two different continuum states, as well as there is no detectable Compton reflection (Smith & Done 1996), which is similar to some states of NGC 4151 (Section 2.4.2).

ACKNOWLEDGMENTS

This research has been supported in part by NASA grants and contracts and the Polish KBN grants 2P03D01008 and 2P03D01410. It has made use of data obtained through the High Energy Astrophysics Science Archive Research Center Online Service, provided by NASA/GSFC. We are especially grateful to C. Done, who provided very valuable comments and suggestions pertaining to this work, as well as supplied us with the *ROSAT* data. Also thanks are due to D. Smith, who provided us with the *Ginga* data, T. Yaqoob, who supplied us with his *ASCA* data files (used in Y95), K. Ebisawa for help with ASCAARF, and Greg Madejski for help with the *ASCA* data reduction.

REFERENCES

Anders E., Ebihara M., 1982, Geochim. Cosmochim. Acta, 46, 2363
Anders E., Grevesse N., 1989, Geochim. Cosmochim. Acta, 53, 197
Antonucci R. R. J., 1993, AAR&A, 31, 473
Arnaud K. A., 1996, in Jacoby G., Barnes J., eds, Astronomical Data Analysis Software and Systems V. The Astron. Soc. of Pacific, in press
Baity W. A., Mushotzky R. F., Worrall D. M., Rothschild R. E., Tennant A. F., Primini F. A., 1984, ApJ, 279, 555
Bałucińska-Church M., McCammon D., 1992, ApJ, 400, 699
Clavel J., et al., 1987, ApJ, 321, 251
Done C., Mulchaey J. S., Mushotzky R. F., Arnaud K. A., 1992, ApJ, 395, 275
Edelson R. A., et al., 1996, ApJ, in press
Evans I. N., Tsvetanov Z., Kriss G. A., Ford H. C., Caganoff S., Koratkar A. P., 1993, ApJ, 417, 82
Finoguenov A., et al., 1995, A&A, 300, 101
George I. M., Fabian A. C., 1991, MNRAS, 249, 352
Gondek D., Zdziarski A. A., Johnson W. N., George I. M., McNaron-Brown K., Magdziarz P., Smith D., Gruber D., 1996, MNRAS, in press
Górecki A., Wilczewski W., 1984, Acta Astron., 34, 141
Gould R. J., Schréder G. P., 1967, PR, 155, 1404
Haardt F., 1993, ApJ, 413, 680
Haardt F., Maraschi L., 1993, ApJ, 413, 507
Haardt F., Maraschi L., Ghisellini G., 1994, ApJ, 432, L95
Halpern J. P., 1984, ApJ, 281, 90
Johnson W. N., et al., 1994, in The Second Compton Symposium, ed. C. E. Fichtel et al. (New York: IAP), 515
Johnson W. N., et al., 1996, in preparation
Jourdain E., Roques J. P., 1995, ApJ, 440, 128
Kaastra J. S., Mewe R., 1993, A&AS, 97, 443
Kriss G. A., Davidsen A. F., Zheng W., Kruk J. W., Espey B. R., 1995, ApJ, 454, L7
Krolik J. H., Kallman T. R., 1984, ApJ, ApJ, 286, 366
Lampton M., Margon B., Bowyer S., 1976, ApJ, 208, 177
Lang K. R., 1974, Astrophysical Formulae (New York: Springer)
Lightman A. P., White T. R., 1988, ApJ, 335, 57
Lightman A. P., Zdziarski A. A., 1987, ApJ, 319, 643 (LZ87)
Lightman A. P., Zdziarski A. A., Rees M. J., 1987, ApJ, 315, L113
Magdziarz P., Zdziarski A. A., 1995, MNRAS, 273, 837
Maisack M., et al., 1993, ApJ, 407, L61
Makishima K., 1986, in Mason K. O., Watson M. G., White N. E., eds, The Physics of Accretion onto Compact Objects. Springer, Berlin, p. 249
McNaron-Brown, K., et al., 1996, in preparation
Morse J., Wilson A. S., Elvis M., Weaver K. A., 1995, ApJ, 439, 121
Nandra K., Pounds K., 1994, MNRAS, 268, 405
Perola G. C., et al., 1986, ApJ, 306, 508
Perotti E., Della Ventura A., Villa G., Di Cocco G., Bassani L., Butler R. C., Carter J. N., Dean A. J., 1981, ApJ, 247, L63
Perotti E., et al., 1991, ApJ, 373, 75
Pounds K. A., Warwick R. S., Culhane J. L., de Korte P. A. J., 1986, MNRAS, 218, 685
Poutanen J., Sikora M., Begelman M. C., Magdziarz P., 1996, ApJ, in press (P96)
Pozdnyakov L. A., Sobol' I. M., Sunyaev R. A., 1983, Ap. Space Phys. Rev., 2, 189
Press W. H., Teukolsky S. A., Vetterling W. T., Flannery B. P., 1992, Numerical Recipes, 2nd Ed., Cambridge Univ. Press
Reilman R. F., Manson S. T., 1979, ApJS, 40, 815
Ross R. R., Fabian A. C., 1983, MNRAS, 261, 74

Shapiro S. L., Lightman A P., Eardley D. M., 1976, ApJ, 204, 187
Smith D., Done C., 1996, MNRAS, 280, 355
Stark A. A., Gammie C. F., Wilson R. W., Bally J., Linke R. A., Heiles C., Hurwitz M., 1992, ApJS, 79, 77
Stern B. E., Poutanen J., Svensson R., Sikora M., 1995, ApJ, 449, L13
Sunyaev R. A., Titarchuk L. G., 1980, A&A, 86, 121
Svensson R., 1984, MNRAS, 209, 175
Svensson R., 1996, A&AS, in press
Tanaka Y., et al., 1995, Nature, 375, 659
Titarchuk L., 1994, ApJ, 435, 570
Titarchuk L., Mastichiadis A., 1994, ApJ, 433, L33 (TM94)
Turner M. J. L., et al., 1989, PASJ, 41, 345
Warwick R. S., Done C., Smith D. A., 1995, MNRAS, 275, 1003 (WDS95)
Warwick R. S., et al., 1996, ApJ, in press
Weaver K. A., Yaqoob T., Holt S. S., Mushotzky R. F., Matsuoka M., Yamauchi M., 1994, ApJ, 436, L27 (W94)
Yaqoob T., Edelson R., Weaver K. A., Warwick R. S., Mushotzky R. F., Serlemitsos P. J., Holt S. S., 1995, ApJ, 453, L81 (Y95)
Yaqoob T., Warwick R. S., 1991, MNRAS, 248, 773 (YW91)
Yaqoob T., Warwick R. S., Makino F., Otani C., Sokoloski J. L., Bond I. A., Yamauchi M., 1993, MNRAS, 262, 435 (Y93)
Yaqoob T., Warwick R. S., Pounds K. A., 1989, MNRAS, 236, 153
Zdziarski A. A., Fabian A. C., Nandra K., Celotti A., Rees M. J., Done C., Coppi P. S., Madejski G. M., 1994, MNRAS, 269, L55
Zdziarski A. A., Ghisellini G., George I. M., Svensson R., Fabian A. C., Done C., 1990, ApJ, 363, L1
Zdziarski A. A., Johnson W. N., Done C., Smith D., McNaron-Brown K., 1995, ApJ, 438, L63
Zdziarski A. A., Lightman A. P., Maciołek-Niedźwiecki A., 1993, ApJ, 414, L93 (ZLM93)
Zdziarski A. A., Magdziarz P., 1996, MNRAS, 279, L21

APPENDIX: OPTICALLY THICK THERMAL COMPTONIZATION

We use the thermal Comptonization model of LZ87 to fit the spectra of NGC 4151. That work uses the Kompaneets equation with a relativistic correction to energy transfer between photons and electrons [eq. (22) in LZ87)]. In the relation between the photon density inside the source and the photon escape rate, LZ87 also take into account reduction at relativistic photon energies of the photon build-up inside the source due to diffusion [eq. (21) in LZ87]. The Kompaneets equation is then solved numerically for an assumed distribution of seed photons, kT, and τ.

LZ87 use a photon-escape probability formalism to obtain the spectra of escaping photons. This implies that the τ used in the Kompaneets equation corresponds to a source with the assumed escape probability. Thus, that τ is geometry-dependent, and it approximately equals the radial optical depth in a uniform sphere. A property of the Kompaneets equation that is geometry-independent is the spectral index of the asymptotic low-energy photon spectrum, α (at energies above those of the seed photons). In the model of LZ87, it equals,

$$\alpha = \left[\frac{9}{4} + \frac{1}{(kT/m_e c^2)\tau(1+\tau/3)}\right]^{1/2} - \frac{3}{2} \qquad (2)$$

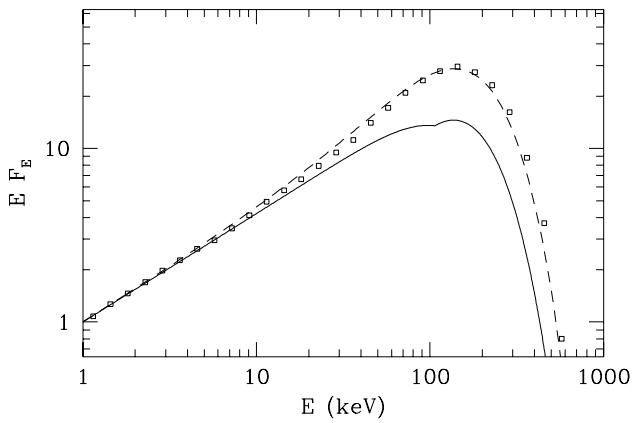

Figure 8. Comparison of Comptonization spectra from a spherical plasma cloud with $kT = 60$ keV, and τ such that the asymptotic low-energy index is $\alpha = 0.38$. Squares represent Monte Carlo results, the solid curve corresponds to the model of Titarchuk (1994) and TM94, and the dashed curve corresponds to the solution of LZ87.

(cf. Sunyaev & Titarchuk 1980). Thus, we use the geometry-independent parameters, α and kT, as the model parameters.

For a specific geometry, we determine the actual optical depth of a source by a Monte Carlo method. The method is based on that of Górecki & Wilczewski (1984). We have tested it in the range of τ from 0.5 to 5 against the corresponding results of Pozdnyakov, Sobol' & Sunyaev (1983) and found excellent agreement.

Fig. 8 shows an example of the (excellent) agreement between the spectra from the Monte Carlo method (squares) and that of LZ87 (dashed curve). The low-energy spectral index is $\alpha = 0.38$, which is imposed for both the solution of the Kompaneets equation and the Monte Carlo spectrum, and $kT = 60$ keV. The optical depth used in the Kompaneets equation is 3.2, whereas the actual τ of a uniform sphere with a uniform distribution of seed photon sources is 3.0. This discrepancy in τ has a negligible practical importance as the derived optical depth is only representative for the astrophysical source of an unknown geometry.

The method of LZ87 formally assumes that the Comptonizing plasma is optically thick. We find that $\tau \gtrsim 2$ (for a sphere) is already sufficient for the validity of the method of LZ87. Fig. 6 in Section 3.1 shows a limiting case with $\tau = 1.3$ ($\alpha = 0.80$ and $kT = 88$ keV for the LZ87 solution), when the assumption of the plasma being optically thick starts to become invalid. We see that then the method of LZ87 still gives an excellent description of the Monte Carlo results (at the same τ), but it overestimates the value of kT, with the actual value from the simulations of $kT = 61$ keV.

Fig. 8 also compares the Monte Carlo results (for $\tau \sim 3$, when the diffusion approximation applies) with those obtained using the solution of Titarchuk (1994; that solution is also published in TM94 and in a few other papers). Titarchuk (1994) also uses the Kompaneets equation, but with a set of relativistic corrections different than those in LZ87. We take $kT = 60$ keV and $\alpha = 0.38$ (corresponding to $\tau = 3.1$) in the solution of Titarchuk (1994). We see

that the spectrum of Titarchuk (1994) underestimates the actual spectrum in the range $E \sim kT$ by a factor of ~ 2. Furthermore, that solution gives an sharp kink around 100 keV, which is clearly unphysical.

The kink appears due to an attempt [eq. (3) in TM94] to account for the relativistic high-energy cutoff steeper than that given by the Wien law [analogous to the diffusion-suppression factor of eq. (21) in LZ87]. For large values of α, equation (3) in TM94 gives indeed a suppression with respect to the low-energy formula [eq. (2) in TM94]. However, the situation reverses at small values of α, when the spectrum without the cutoff correction is already below the correct spectrum, and a hump appears in the spectrum above the kink, see Fig. 8. Concluding, the model of Titarchuk (1994) and TM94 may introduce large errors in fitting Xγ data.